ARCHIVES OF TRANSPORT *ISSN (print):* *0866-9546*
Volume 78, Issue 2, 2026 ***e-ISSN (online):*** *2300-8830*
DOI: *10.61089/aot2026.x9pzyp23*

ENHANCING THE RESILIENCE OF THE BELT AND ROAD SEA-RAIL MULTIMODAL TRANSPORT NETWORK: A CRITICAL NODE IDENTIFICATION METHOD INTEGRATING CYCLE STRUCTURE AND PERSISTENT HOMOLOGY

Youpeng LU[1], Xiaowei CHEN[2], Fan CHEN[3]

[1, 2] *School of Traffic and Transportation, Lanzhou Jiaotong University, Lanzhou, China*
[3] *Faculty of Geomatics, Lanzhou Jiaotong University, Lanzhou, China*

***Abstract**:*

Key node identification in multimodal transportation networks is essential for improving operational efficiency, mitigating risk propagation, and enhancing network resilience. However, traditional centrality metrics often fail to capture the higher-order topological support roles and multi-scale structural persistence of nodes in coupled multimodal networks. To address this limitation, this paper proposes CPHD (Cycle Persistent Homology – Degree), a node importance metric integrating cycle-structure persistent homology with node degree information. Specifically, a cycle-oriented multi-scale filtration process is constructed within the first- and second-order neighborhoods, where a Dowker filtration based on Jaccard topological distance extracts the persistent features of triangular (3-cycle) structures, and a Vietoris–Rips filtration based on shortest-path distance captures the persistence of quadrilateral and pentagonal cycles. The multi-scale persistent homology values are fused into a Cycle Persistent Homology value with weights determined by the entropy weight method, then multiplicatively aggregated with the normalized node degree, jointly capturing higher-order structural support and local connectivity. Comparative experiments on four real-world networks indicate that CPHD achieves the best overall performance among the compared metrics, including Degree Centrality, Betweenness Centrality, Closeness Centrality, K-core, and Cycle-Ratio, in terms of structural disruption capability, propagation consistency, and ranking differentiation: it yields the fastest giant-connected-component decline, the lowest robustness values in most networks, and the highest Kendall's Tau correlation with SIR-based spreading influence rankings across most infection probabilities. A case study on the Belt and Road sea–rail multimodal transportation network, a dual-layer coupled network with 201 nodes and 448 edges, demonstrates the effectiveness and interpretability of CPHD. Removing about 13% of the top-ranked nodes reduces the largest connected component and global network efficiency to below 10% of their initial levels, and CPHD identifies not only maritime hubs such as Singapore and Kaohsiung and railway border stations such as Alataw and Khorgos, but also cross-system coupling nodes such as Shanghai and Shekou. The results indicate that CPHD provides a reliable and interpretable framework for identifying structurally critical nodes in multimodal transportation networks, offering a topology-based quantitative reference for resilience enhancement and critical infrastructure protection.

Keywords: *sea-rail intermodal transportation, complex networks, network resilience, key node identification, cycle persistent homology*

To cite this article:

Lu, Y., Chen, X., Chen, F. (2026). Enhancing the resilience of the belt and road sea-rail multimodal transport network: A critical node identification method integrating cycle structure and persistent homology. Archives of Transport, 78(2), 171-195. https://doi.org/10.61089/aot2026.x9pzyp23

Contact:
1) youpenglu@mail.lzjtu.cn [https://orcid.org/0000-0002-8310-1194] – corresponding author; 2) 2991156194@qq.com [https://orcid.org/0009-0005-7986-3152]; 3) chenfan@mail.lzjtu.cn [https://orcid.org/0000-0002-4775-7065]

Article is available in open access and licensed under a Creative Commons Attribution 4.0 International (CC BY 4.0)

1. Background and Motivation

The Belt and Road Initiative (BRI), as a strategic platform for China to promote global connectivity, aims to achieve shared prosperity and development by strengthening infrastructure construction and economic cooperation among countries along the routes. The sea-rail multimodal transport network serves as a critical link enhancing cross-regional cargo efficiency and international trade. However, amid profound geopolitical shifts—including the Russia-Ukraine war and Iran's Strait of Hormuz blockade—the security and resilience of key logistics corridors have become increasingly vital for national economic security and global supply chain stability(B. Chen et al., 2026).

As a highly coupled complex system, the sea-rail multimodal transport network relies on seamless integration and efficient coordination among multiple transport modes for stable operation. While such cross-system synergy improves transport efficiency, it also amplifies systemic risks under extreme disruptions. Rail transport depends on fixed routes and nodes; once critical corridors are blocked, short-term rapid reconfiguration through alternative paths is difficult(Yiqiao, Xianbin, Fangyun, & Lu Carol, 2022). Although sea systems possess high capacity and flexibility, disruptions to key waterways or hub ports often exhibit cascading effects with trans-regional diffusion(K. Xu, Liu, & Li, 2025). When vulnerabilities from different transport subsystems overlap in the multimodal network, local interruptions can rapidly evolve into system-wide functional degradation or even network-wide paralysis(Chao Zhu & Zhu, 2024). Precisely identifying core nodes bearing critical structural functions and implementing targeted interventions has become a key strategy to enhance the stability and resilience of multimodal transport networks.

Traditional methods typically focus on single transport systems or localised frameworks, failing to capture complex higher-order topological information in multimodal transport networks. In highly coupled multi-subsystem networks, they tend to overlook nodes that, despite low connectivity, play irreplaceable roles in maintaining local synergy, providing path redundancy, and suppressing disruption propagation(X. Huang, Chen, Cai, Wang, & Hu, 2022). In response, this paper proposes CPHD (Cycle Persistent Homology–Degree), a node importance metric integrating persistent homology of cycle structures with node degree information, to more accurately identify key nodes supporting structural integrity and resilience in complex transport networks.

2. Literature Review and Research Gap

Complex network theory provides an important analytical framework for critical node identification in transportation systems(W. Huang et al., 2024). With the development of data acquisition and modeling methods, complex network analysis has been widely applied to resilience assessment and critical node identification in transportation systems such as highways, railways, aviation, and sea transport, offering operational quantitative bases for transportation organization optimization, infrastructure protection, and system resilience enhancement(X. Xu & Xu, 2024).

Sorting node importance based on network topological properties is currently the mainstream method for critical node identification. From degree centrality (DC)(Chang & Kim, 2022), which reflects the scale of node connections, to closeness centrality (CC)(Li, Teng, & Wang, 2025), which measures the proximity of a node to others, and to betweenness centrality (BC)(Guo, Zhao, & Gao, 2026), which characterizes a node's mediating role in the entire network, these methods have all provided effective means for critical node identification. However, most of these methods focus on single networks and typically characterize node importance from a single topological dimension, emphasizing local connectivity features or low-order structural properties. This makes it difficult to fully reveal the true role of nodes in the overall structural organization and functional maintenance of complex transportation networks(Liu, Tian, Huang, & Yang, 2018).

As research on multimodal transport networks deepens, studies have begun to address the network complexity arising from the coupling of multiple transportation modes, attempting to identify critical nodes from perspectives such as overall organization, cross-modal connectivity, and integration of multi-dimensional attributes(Gao, Hu, Yang, & Zhao, 2024; Stamos, 2023). Some studies have constructed directed weighted networks integrating sea, air, rail, and road transport, proposing various centrality metrics to identify key transportation cities(Shen & Zong, 2023). Others have combined im-

proved TOPSIS, grey relational analysis, and information entropy weighting methods to achieve comprehensive critical node identification in multi-layer heterogeneous transportation networks(Zhang & Ng, 2021). Although these studies expand the application boundaries of traditional methods, they generally remain at the level of comprehensive evaluation of node and edge attributes, still insufficiently characterizing higher-order topological structures of networks.

To break through the limitations of low-order topological descriptions, some research has started to focus on the role of higher-order topological features such as cycle structures, motifs, and other structural patterns in node importance identification(J. Chen, Wang, Xia, Shi, & Chen, 2025; Fan, Lü, Shi, & Zhou, 2021). Studies show that node importance in complex networks is not only influenced by local connectivity features and shortest path distributions but is also closely related to higher-order topological structures(Lambiotte, Rosvall, & Scholtes, 2019; Y. Xu, Zhao, Chen, Liu, & Xia, 2024). For multimodal transport networks, such higher-order structures can more fully reflect closed associations, alternative paths, and collaborative organizational mechanisms between different transportation modes. Based on this understanding, the Cycle Ratio (CR) metric has been proposed(Fan et al., 2021). This metric characterizes the degree of node participation in cycle structures through a cycle count matrix, emphasizing a node's participation level in cycle structures and its contribution to neighborhood structure and overall network organization. To some extent, it compensates for the inadequacy of low-order topological metrics in characterizing complex structural relationships, providing ideas for identifying critical nodes from a higher-order topological perspective.

However, current research on critical node identification in multimodal transport networks faces two key limitations. First, while some studies incorporate higher-order features like cycle structures, they remain at combined node–edge evaluation levels, with insufficient exploration of higher-order patterns, local topological nesting, and multi-scale organisation. Second, most methods rely on static networks—whether low-order (DC, BC) or higher-order (CR) metrics—focusing on fixed-state structures while neglecting the persistence and evolutionary stability of local topological features across scales. For multimodal networks with complex couplings and abundant alternative paths, node importance depends not only on participation in key structures but also on the persistence and stability of supported structures across scales. This highlights the need for methods combining higher-order topological characterisation with dynamic persistence analysis.

Based on this, this paper proposes CPHD, a critical node identification method leveraging persistent homology features of cycle structures. Combining node degree as a low-order feature with a cycle-oriented multi-scale filtration and persistent homology analysis, CPHD extracts second-order neighborhood features reflecting the persistence of higher-order topological structures. These are fused with low-order attributes to form a comprehensive ranking metric that captures both local connectivity and persistent roles in higher-order structures, offering new methodological support for multimodal transport networks. The main contributions are:

1. Constructing a cycle-oriented filtration process within the second-order neighborhood. By applying cycle-oriented multi-scale filtration with persistent homology analysis, multi-scale persistent cycle features are extracted from the second-order neighborhood, precisely reflecting a node's structural role in local higher-order topology and enhancing critical node identification in complex coupled networks.
2. Establishing a framework integrating higher-order topological persistence features with low-order local attributes. By combining higher-order structural information with node degree, the ranking simultaneously reflects a node's higher-order structural support role and local connectivity, addressing the limitations of single static low-order metrics and providing a more comprehensive approach for critical node identification in multimodal transport networks.
3. Validating the effectiveness and applicability of the proposed method through comparative experiments on multiple real-world networks and a case study of the Belt and Road sea-rail multimodal transport network.

The remainder of this paper is organized as follows. Section 3 presents the cycle structure persistent homology-based node importance evaluation method and its implementation process. Section 4 conducts comparative experiments on multiple real-world networks to verify the method's effectiveness and ro-

bustness in general complex networks. Section 5 examines the method's applicability in real multimodal transport scenarios through the Belt and Road sea-rail multimodal transport network case. Finally, Section 6 concludes the paper.

3. Critical Node Identification Method Based on Cycle Structure Persistent Homology Values

3.1. Cycle Structure

In complex networks, cycle serve as a critical component for characterising higher-order topological features and act as fundamental structural units reflecting the network's closed connectivity relationships, alternative paths, and local collaborative organisational mechanisms. A cycle of length l is represented as an ordered node sequence$v_1, v_2, \ldots, v_l$, where for any i $(1 \le i \le l)$, node v_i is adjacent to v_{i+1}, and the terminal nodes v_1 and v_l are also adjacent. Triangles represent the most basic cycle structures. Cycle structures enhance network connectivity and robustness by introducing redundant paths, offering greater resilience to failures than chain or star configurations.

In sea-rail multimodal transport networks, multiple interacting nodes form various cycle structures that contribute differently to network resilience. Triangles (3-cycles) represent the most fundamental redundancy unit, formed when two neighbors of a common node are directly linked, providing the shortest alternative path. Quadrilaterals (4-cycles) add a fourth node to extend detouring capacity under failures. Pentagons (5-cycles) and larger cycles exist but require more interactions and yield weaker cohesion. To balance topological expressiveness and computational cost, , topological feature extraction is restricted to 3-cycles, 4-cycles, and 5-cycles—that is, triangles, quadrilaterals, and pentagons—which the algorithm enumerates explicitly. Cycles of length greater than 5 are not enumerated individually; their influence is reflected indirectly through the persistence of lower-order structures.

However, their significance lies not merely in existence but in persistent presence across scales, which is critical for capturing their true structural importance in multimodal transport networks. As illustrated in Figure 1, nodes A and B each contain only one quadrilateral cycle within their second-order subgraphs; relying solely on cycle count fails to distinguish their topological contributions. To address this limitation, we compute persistent homology values of cycle structures in the second-order subgraph. Figure 2 shows that the 1-dimensional cycle of node A is born at filtration threshold 2.0, whereas that of node B is born at threshold 3.0. Since no maximum threshold is set, no death time is recorded. Compared with raw cycle counts, persistent homology values provide greater discriminability by capturing the multi-scale birth information of cycle structures, thereby offering a more expressive characterization of high-order topological features.

3.2. Persistent Homology

In persistent homology, topological data is represented not by a single simplicial complex but by a nested sequence constructed via a filtration function. This enables computing homology group variations across parameters, thereby characterising the persistence of topological features. For each simplicial complex K in the family of simplicial complexes $\mathscr{F}_i$, the q -dimensional homology groups $H_q(K)$ are computed, yielding the persistent homology results.

$$H_q(\mathscr{F}_i) = \left\{H_q(K_\delta) \to H_q(K_{\delta'})\right\}_{0 \le \delta \le \delta'} \tag{1}$$

Specifically, the appearance and disappearance times of each topological structure within the family of simplicial complexes are represented as barcodes:

$$Pers_q(\mathscr{F}_i) = \left\{(b_{i,j}, d_{i,j}) \in [0, \delta_m] \times [0, \delta_m] \middle| b_{i,j} < d_{i,j}, j \in \mathbb{N}^+, j \le J_{q,i}\right\} \tag{2}$$

Herein, b denotes the birth time of the topological structure, while d denotes its death time. $J_{q,i}$ represents the count of q -dimensional homology groups. For certain topological structures that persist indefinitely after birth, their death time is conventionally set to the maximum value of the filtration parameter, δ_m, during computation.

To specifically identify cycle structures at different scales, distinct filtration functions are required to filter node neighbor subgraphs. For the 1-hop neighbor subgraph $G_i^1 (1 \le i \le n)$, the Dowker filtration function is applied, yielding the Dowker complex cluster $F_i^D = \left\{D_{\delta_1}, D_{\delta_2}, \ldots, D_{\delta_m}\right\}$, where $D_{\delta_1} \subseteq D_{\delta_2} \subseteq \cdots \subseteq D_{\delta_m}$, and the filtration parameter δ satisfies $\delta_1 < \delta_2 < \cdots < \delta_m$. Similarly, for the 2-hop neighbor subgraph $G_i^2 (1 \le i \le n)$, the VR filtration function is utilized, resulting in the VR complex cluster $F_i^{VR} = \left\{Cl(G_{i,\delta_1}^2), Cl(G_{i,\delta_2}^2), \ldots, Cl(G_{i,\delta_m}^2)\right\}$.

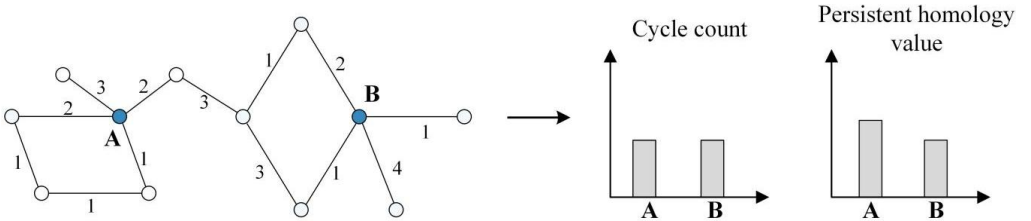


Fig. 1. Schematic of different high-order topological features

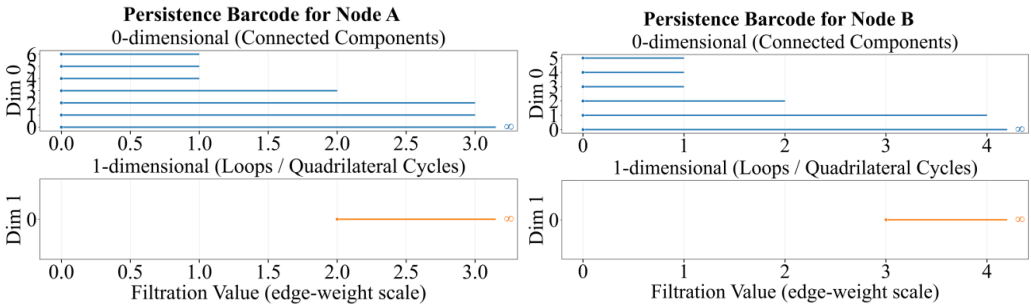


Fig. 2. Persistence barcode diagram

3.2.1. Dowker Filtration Function

The Dowker filter function identifies triangular structures in network subgraphs(Ye, Jiang, Jiang, & Li, 2023). To incorporate local topology into persistent homology, we introduce a topological distance based on Jaccard similarity and construct the corresponding filtration process(Bag, Kumar, & Tiwari, 2019). Specifically, for any pair of nodes, v_i and v_j, in the graph, their topological distance S_{ij} is defined as:

$$PS_{ij} = 1 - \frac{|N(v_i) \cap N(v_j)|}{|N(v_i) \cup N(v_j)|} \tag{3}$$

Where, $N(\cdot)$represents the neighbourhood set of a node. This distance metric quantifies topological dissimilarity between node neighbourhoods: more common neighbours yield shorter distances. During filtration, basic cycle structures form preferentially. By defining the topological distance S_{ij} as a weight function $W_1: E \to \mathbb{R}$ on the edges, the unweighted undirected network G is transformed into an undirected weighted network $G_1 = (V, E, W_1)$. If there exists a target node $v' \in V$ such that for any $v_i (1 < i < n)$, $W(v_i, v') \leq \delta$, then we have the Dowker q -sink complex $\mathfrak{D}_\delta^{si} = \{\sigma = [v_1, v_2, \cdots, v_n]\}$, and based on this, the Dowker sink filtration is defined as $\left\{\mathfrak{D}_\delta^{si} \to \mathfrak{D}_{\delta'}^{si}\right\}_{0 \leq \delta \leq \delta''}$. Correspondingly, if there exists a node $v' \in V$ such that for any $v_i (1 \leq i \leq n)$, $W(v', v_i) \leq \delta$, then we have the Dowker q -source complex $\mathfrak{D}_\delta^{so} = \{\sigma = [v_1, v_2, \cdots, v_n]\}$, and the Dowker source filtration is denoted as $\left\{\mathfrak{D}_\delta^{so} \to \mathfrak{D}_{\delta'}^{so}\right\}_{0 \leq \delta \leq \delta''}$. Triangular cycle structures in complex network systems can be formed in multiple ways. Using the Dowker filtration defined on unweighted undirected networks, without distinguishing between source nodes and target nodes, the n neighbouring nodes of a single node are combined to form an $(n-1)$ -dimensional simplex. The filtration process is illustrated in Figure 3. Specifically, when $\delta \leq 1$, the two neighboring nodes E and G of node F form a 1-simplex, while nodes A and D each constitute a 0-simplex. When$\delta \leq 3$, nodes B, C, and D share a common neighbor node A, thus forming a 2-simplex; in contrast, nodes F, G, and H have no common neighbor node, thereby yielding a 1-dimensional cycle structure.

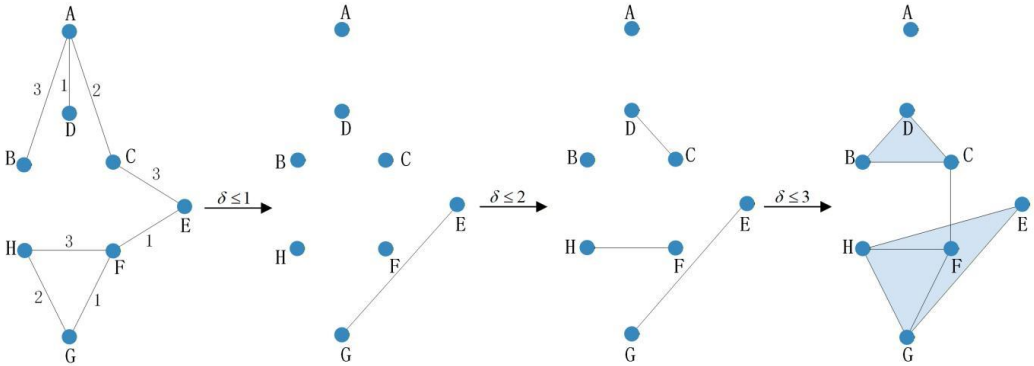


Fig. 3. Schematic diagram of Dowker filter filtration process

3.2.2. VR Filtration Function

The VR filter function is utilized to identify cycle structures in network subgraphs other than triangles(Lim, Memoli, & Okutan, 2024). By defining the shortest-path distance d_{ij}^{Cl} in the network as a weight function $W_2: E \to \mathbb{R}$ on the edges, the network G is transformed into $G_2 = (V, E, W_2)$. Unlike triangles, which emphasize direct neighborhood overlap, quadrilaterals and pentagons represent indirect connectivity and detour capacity—key structural resilience attributes in transportation networks. Shortest-path distance directly measures the connectivity cost between nodes, serving as the canonical metric for evaluating rerouting efficiency and path diversity(Latora & Marchiori, 2001). This choice ensures that our VR filtration captures the persistence of structurally alternative paths that maintain network functionality under disruptions. For any $\delta \in R$, let the subnetwork be $G_\delta = (V, E, W_\delta) \subset G$, where the edge set $E_\delta \in E$ contains only edges with weights less than or equal to δ. Then, for any $\delta \in R$, the VR complex is defined as the clique complex $Cl(G_\delta)$ of the subnetwork G_δ, and the VR filtration is defined as $\{Cl(G_\delta) \to Cl(G_{\delta'})\}_{0 \le \delta \le \delta'}$. The clique complex $Cl(G)$ is a simplicial complex in which each simplex corresponds to a complete subgraph in G. During this filtration process, the set of nodes is first added to the VR complex. Subsequently, as the parameter δ varies, edges are incorporated into complete subgraphs in ascending order of their weights. Throughout this process, the VR filtration structure gradually takes shape, as illustrated in Figure 4.

In Figure 4, when $\delta \le 1$, nodes A, B, and C are connected to form a connected component, reducing the total number of connected components from 5 to 3. When $\delta \le 3$, nodes A, B, C, D, and E form a 5-cycle structure, which further evolves into a 4-cycle structure when$\delta \le 4$. By recording the persistence of cycle structures across different scales, these persistent features can be extracted as high-order topological features of the nodes.

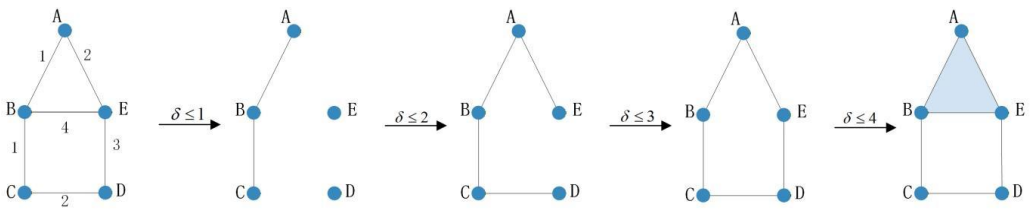


Fig. 4. Schematic diagram of VR filter filtration process

3.3. Calculation of Persistent Homology Values for Cycle Structures

First, let us consider an undirected and unweighted network denoted as $G = (V, E)$, where $V = \{v_1, v_2, \cdots, v_n\}$ represents the set of nodes in the network, with n indicating the total number of nodes; and $E = \{e_1, e_2, \cdots, e_m\}$ represents the set of edges in the network, with m being the total number of edges. The adjacency matrix of this network is $A_{n\times n} = (a_{ij})$, where $a_{ij} = 1$ if there is an edge connecting node v_i and node v_j, and $a_{ij} = 0$ otherwise.

In this paper, we adopt the homology characteristics of cycle structures at different scales within first- and second-order neighbor subgraphs as high-order topological features of nodes. The extraction process of high-order topological features for nodes is illustrated in Figure 5. The Cycle Persistent Homology Value (CPH) is obtained by summing the existence durations of topological structures for each node, as follows:

$$CPH_q(v_i) = \sum_{j=1}^{J_{q,i}} (d_{i,j} - b_{i,j}) \tag{4}$$

When setting $q = 1$, we can calculate the homology characteristics $CPH_q(v_i)$ of 1-dimensional holes near node v_i. The Dowker homology characteristics $CPH_{\triangle}^{Dowker_i}$ calculated using $\mathscr{F}_i^D$ correspond to the high-order topological features of various triangular cycle structures near node v_i. Similarly, the VR homology characteristics $CPH_{4\text{-cycle}}^{VR}(v_i)$ and $CPH_{5\text{-cycle}}^{VR}(v_i)$ calculated using $\mathscr{F}_i^{VR}$ correspond to the high-order topological features of cycle structures (other than triangles) near node v_i. A larger persistent homology value implies that the topological structure persists for a longer duration during the filtration process, indicating a more enduring functional role of the topological structure and more prominent high-order topological features.

Although high-order features reveal cycle participation and path redundancy, relying solely on them has limitations. As shown in Figure 6, using only high-order features (e.g., cycle counts) assigns node A (no cycles) a score of 0, while nodes B and C receive similar scores despite C having greater actual influence due to stronger local connectivity. Conversely, using only low-order features like degree centrality assigns high scores to A and C, underestimating node B. Thus, neither low-order nor high-order features alone can comprehensively capture node importance.

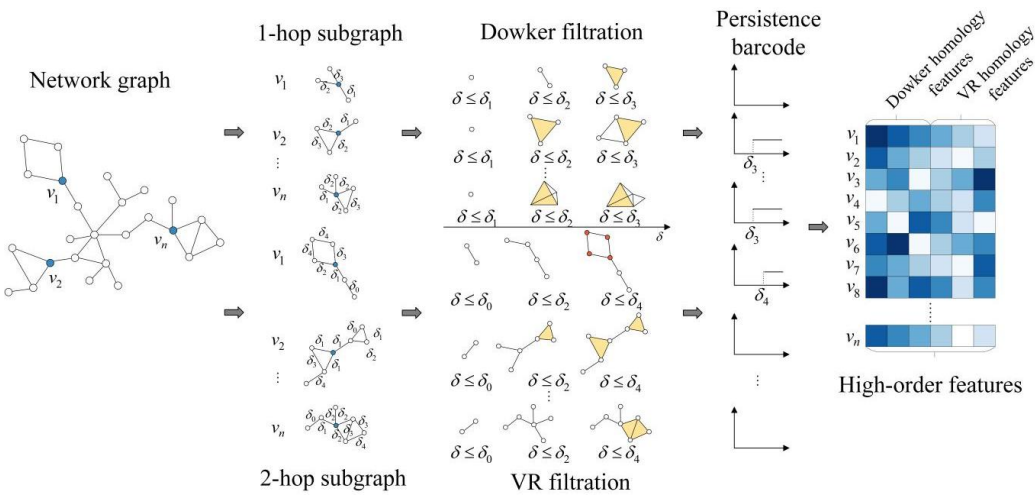


Fig. 5. Schematic diagram of node high-order topological feature extraction

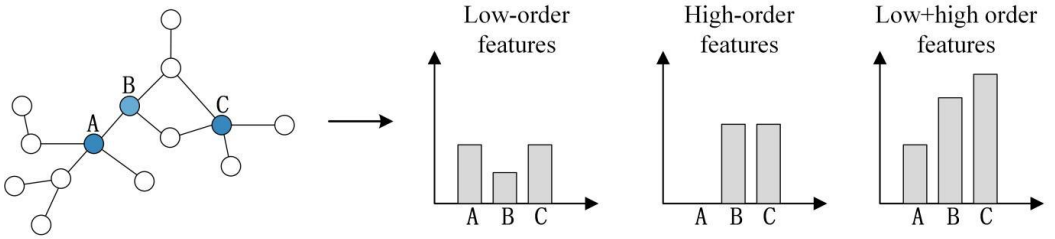


Fig. 6. Schematic illustration of node importance differentiation using low-order and high-order topological features

To quantify the influence of neighboring nodes on the evaluated nodev_i, we incorporate the node degree value D into the node evaluation metric $CPH(v_i)$. This enables the metric to not only depict the node's supporting role within local high-order structures but also reflect its neighboring connectivity capabilities, thereby achieving a more comprehensive and nuanced identification of key nodes. For an undirected and unweighted network, the node importance identification method based on the cycle persistent homology-degree is denoted as $CPHD(v_i)$. Specifically, the CPHD-index for node v_i is computed by multiplicatively aggregating the persistent homology value of cycles with the node degree as follows:

$$CPHD(v_i) = \frac{d(v_i) - d_{min}}{dmin_{max} \times CPH(v_i)} \quad (5)$$

Here, $CPH(v_i)$ denotes the higher-order topological feature value of node a, which is fused from the one-dimensional homology values of triangle (3-cycle), quadrilateral (4-cycle), and pentagonal (5-cycle) cycle structures within the neighborhood of nodev_i. Specifically, 3-cycle structures are extracted via the Dowker filtration, while 4-cycle and 5-cycle structures are extracted via the Vietoris-Rips (VR) filtration. To integrate these high-order topological features with the conventional degreecentrality, the degree value of each node is first normalized to the range [0,1] using min-max normalization, ensuring that both the degree and topological feature components are on a comparable scale and that neither dominates the aggregation due to magnitude differences. The multiplicative form ensures that they are jointly indispensable: if either the persistent homology value or the normalised degree is zero, the CPHD value vanishes, reflecting a semantic requirement that a critical node must simultaneously possess high structural redundancy, as characterised by persistent homology, and high connectivity, as characterised by its degree. The weights of features at different scales are objectively determined by the entropy weight method according to their distribution differences across all nodes in the network, providing a data-driven balance among the components and avoiding subjective parameter tuning: the information entropy of each feature is first calculated; the smaller the entropy, the greater the internode difference and discriminative ability of the feature, and thus the higher the assigned weight; conversely, features with larger entropy receive lower weights(W. Huang et al., 2021). The specific steps are outlined in Algorithm 1.

CPHD constructs multi-scale filtrations within the second-order neighborhood, extracting persistent cycle features and integrating them with degree information. This simultaneously captures path redundancy and local connectivity, addressing traditional centrality metrics' limitations in depicting high-order loop information. This makes CPHD particularly suited for multimodal transport networks, effectively representing circulation structures formed by cross-mode interweaving and cross-system dependencies.

Algorithm 1 *CPHD-Based Node Importance Evaluation Framework*

Input: Graph $G = (V, E)$
Output: CPHD values for all nodes in V
procedure CPHD($v, G, w, dmax_{min}$
  Extract 1-hop neighbors $N_1(v)$
  Extract 2-hop neighbors $N_2(v)$
  Construct induced subgraph G_v
  Compute shortest-path distance matrix M
  Replace infinite distances by a large constant
  $CPH_1^{Dowker\text{Dowker}_v}$
  $\{CPH_1^{VR}(v) | CPH_{4-\text{cycle}}^{VR}(v), CPH_{5-\text{cycle}}^{VR}(v)\} \leftarrow \text{VR}(v, G_v)$
  Apply sigmoid function $\sigma(x) = \frac{1}{1+e^{-x}}$
  Compute the high-order topological features of node v
  $\boldsymbol{CPH_1(v) = w_1 \times \sigma\left[CPH_{\triangle}^{Dowker}[]_2[CPH_{4-\text{cycle}}^{VR}(v)]_3[CPH_{5-\text{cycle}}^{VR}(\right.}$
  Compute normalized degree:
  $\hat{d}(v) = \frac{d(v)-d_{min}}{dmin_{max}}$
  return
  $\boldsymbol{CPHD(v) = \hat{d}(v) \times CPH_1(v)}$
end procedure
procedure Dowker(v, G_v)
  Initialize similarity matrix S
  for each node pair (v_i, v_j) in G_v **do**
    $N_{ij} \leftarrow \frac{|N_1(v_i) \cap N_1(v_j)|}{|N_1(v_i) \cup N_1(v_j)|}$
  end for
  Convert similarity matrix to distance matrix $D_s = 1 - N$
  Extract 1-dimensional persistence intervals
  return CPH_1^{Dowker}
end procedure
procedure VR(v, G_v)
  $\mathscr{R} \leftarrow VR(M, maxdim = 1, \text{do_cocycles=True})$
  dgms $\leftarrow \mathscr{R}$.cocycles[1]
  Initialize $CPH_{4\text{-cycle}} \leftarrow 0$, $CPH_{5-\text{cycle}} \leftarrow 0$
  for each persistence interval $(b, d) \in dgms[1]$ **do**
    $p \leftarrow d - b$
    $c \leftarrow$ cocycle corresponding to (b, d)
    $E_{\text{support}} \leftarrow \{(i, j) | c(i, j) \neq 0\}$
    L_{min}
    for each edge $(u, v) \in E_{\text{support}}$ **do**
      if a shortest path P from $\boldsymbol{u}$ to $\boldsymbol{v}$ exists in $\boldsymbol{N_2(v)}$ **then**
        $\boldsymbol{L \leftarrow |P| + 1}$
        $L\,min(_{min_{min}}$
      end if
    end for
    if L_{min} **then**
      $CPH_{4-\text{cycle}} \leftarrow CPH_{4-\text{cycle}} + p$
    else if L_{min} **then**
      $CPH_{5\text{-cycle}} \leftarrow CPH_{5\text{-cycle}} + p$
    end if
  end for
  return $(CPH_{4\text{-cycle}}, CPH_{5\text{-cycle}})$
end procedure
procedure Compute weights $\boldsymbol{w}$
  Construct feature matrix $X \in \mathbb{R}^{n \times 3}$, where columns correspond to $CPH_{\triangle}^{Dowker}$, $CPH_{4-\text{cycle}}^{VR}$, $CPH_{5-\text{cycle}}^{VR}$
  for $j = 1$ to 3 **do**
    $S_j \leftarrow \sum_{i=1}^{n} x_{ij}$
    for $i = 1$ to n **do**
      $q_{ij} \leftarrow \frac{x_{ij}}{S_{ij}}$
    end for
  end for
  for $j = 1$ to 3 **do**
    $e_j \leftarrow -\frac{1}{ln\,n} \sum_{i=1}^{n} q_{ij}\, ln\, q_{ij}$
    $h_j \leftarrow 1 - e_j$
  end for
  $H \leftarrow \sum_{j=1}^{3} h_{ij}$
  for $j = 1$ to 3 **do**
    $w_j \leftarrow \frac{h_{ij}}{H}$
  end for
  return $w = (w_1, w_2, w_3)$
end procedure
Compute degree bounds ($dmax_{min}$
for each node $v \in V$ **do**
  $CPHD(v) \leftarrow$ CPHD($v, G,$ w, $dmax_{min}$
end for
return $\{CPHD(v)\}_{v \in V}$

4. Experiments and Results

4.1. Experimental Network

To verify the effectiveness and applicability of the proposed node importance identification method in general complex networks, this paper selects four real-world networks from different domains for comparative analysis, including: (a) Drug(Correia, de Araújo Kohler, Mattos, & Rocha, 2019), (b) Adjnoun(Newman, 2006), (c) Friendship-3(Chami, Ahnert, Kabatereine, & Tukahebwa, 2017), and (d) Paris(Crucitti, Latora, & Porta, 2006). The topological structures of these networks are illustrated in Figure 7.

In these example networks, key node definitions vary: in the Drug network, they represent drugs prone to triggering extensive interactions; in the Adjnoun network, they denote adjectives serving as structural, thematic, or emotional cores. Despite these differences, all networks are abstracted as undirected, unweighted topological networks with self-loops removed, ensuring consistent evaluation criteria. Basic statistics are presented in Table 1, where N and E denote the number of nodes and edges in the network, respectively; $\langle k \rangle$ represents the average degree; L represents the average path length; C indicates the average clustering coefficient; and r signifies the assortativity coefficient.

The selected networks exhibit significant variations in foundational statistical characteristics, confirming their representativeness of diverse real-world structures. For instance, the Paris network has the lowest average degree (2.9382) and clustering coefficient (0.0472), indicating a sparse structure with low node aggregation, whereas the Friendship-3 network has the highest average degree (11.1033), reflecting denser connectivity, and the Adjnoun network has the highest clustering coefficient (0.1903), indicating stronger node clustering tendencies.

.2. Connectivity Validation Analysis

In node importance evaluation, connectivity validation analysis serves as a core method for validating the effectiveness of node ranking results(Y. Huang, Wang, Ren, & Lü, 2024). Connectivity validation analysis involves progressively removing nodes from the network based on their importance rankings provided by different metrics, while simultaneously monitoring changes in the size of the network's giant connected component (GCC). These changes are used to assess the network's ability to maintain connectivity. Additionally, to more comprehensively compare the performance differences among various methods during the removal of critical nodes, this paper introduces the R -value as a test parameter for network robustness. The formula for calculating the R -value is as follows:

$$R = \frac{1}{N}\sum_{n=1}^{N} g(n) \tag{6}$$

Where, $g(n)$ is the relative size of the largest connected component after the removal of n nodes and N is the initial number of nodes. The normalization factor $\frac{1}{N}$ eliminates the influence of network size, so that the resulting R values can be compared directly across networks of different sizes and across different attack strategies. A smaller R -value indicates that when the same proportion of nodes are removed, the network's connectivity declines more rapidly, meaning that the corresponding method is more effective in identifying nodes that play a crucial supporting role in the network.

Figure 8 presents four real-world networks ranked by seven metrics—DC, BC, CC, K-core, CR, Random, and the proposed CPHD—with GCC changes during node removal compared in Figure 8. For the random attack, the simulation is repeated 10 times at each removal fraction with independent random node selections, and the reported curve is the mean of the GCC size over the 10 repetitions. The CPHD-based ranking yields the fastest GCC decline, reducing the giant connected component to below 10% of its original size before 50% of nodes are removed, indicating that CPHD-identified nodes exert the most significant destructive effect on network connectivity.

Table 1. Four basic topological characteristics of real networks

Network name	N	E	$\langle k \rangle$	L	C	r
Drug	75	181	4.7271	2.8131	0.1571	-0.3146
Adjnoun	112	425	7.4746	2.5354	0.1903	-0.1293
Friendship-3	192	1181	11.1033	2.4440	0.1574	-0.0842
Paris	335	494	2.9382	11.3237	0.0472	0.0107

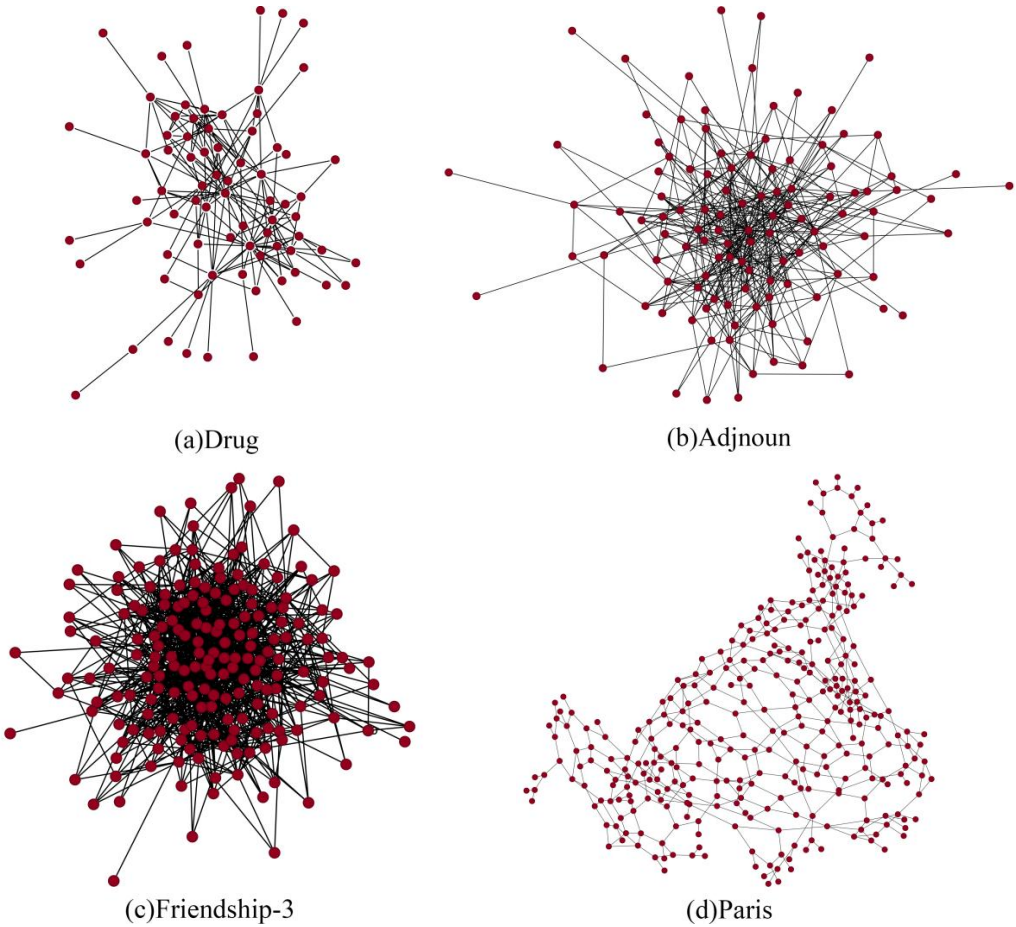


Fig. 7. Diagram of network topological structure

In contrast, the important nodes identified by traditional centrality metrics (DC, BC, CC, K-core) and the cycle-ratio metric (CR) tend to exhibit a relatively weaker destructive effect on overall network connectivity. Specifically, when 50% of the nodes are sequentially removed based on these metrics, the giant connected component generally retains a size of 30%–50%. Notably, CR consistently outperforms CC and K-core across all four networks, confirming the value of incorporating cycle structure information; however, it remains less effective than CPHD, suggesting that raw cycle counts capture only partial high-order topological information. Moreover, in the Paris network, which possesses the lowest node clustering degree as illustrated in Figure 8(d), this phenomenon becomes particularly pronounced: certain nodes ranked as important by the CC and K-core metrics are even less critical than randomly selected nodes, whereas both CR and CPHD maintain consistent effectiveness, further highlighting the limitations of conventional approaches in capturing structurally vulnerable nodes within sparsely clustered topologies.

This is attributable to the fact that traditional centrality metrics typically place emphasis on the local connection characteristics or positional attributes of nodes, while overlooking the role of nodes in maintaining connectivity between different regions. Although CR incorporates cycle structure information, it treats all cycles equally regardless of their multi-

scale stability, thereby missing the nuanced topological persistence that distinguishes critical from non-critical cycles. In contrast, the CPHD metric integrates local connection information with persistent homology-based high-order structural features, enabling it to more precisely identify nodes that play a pivotal supporting role in the overall connectivity of the network. Table 2 presents the R-values of the four real-world networks under the seven different metrics. It can be observed that the R-value of CPHD is only marginally higher than that of DC in the Drug network (0.1697 vs. 0.1670), and it is the lowest among the remaining metrics across the other three networks. The CR metric exhibits a consistent middle-tier performance, ranking fourth among the seven metrics in all four networks. While CR outperforms CC and K-core universally—demonstrating the incremental value of cycle structure information—its R-values remain higher than those of CPHD across all networks, quantitatively confirming that persistent homology values provide more discriminative high-order topological features than raw cycle counts. This further underscores the effectiveness and applicability of identifying important nodes based on the CPHD metric.

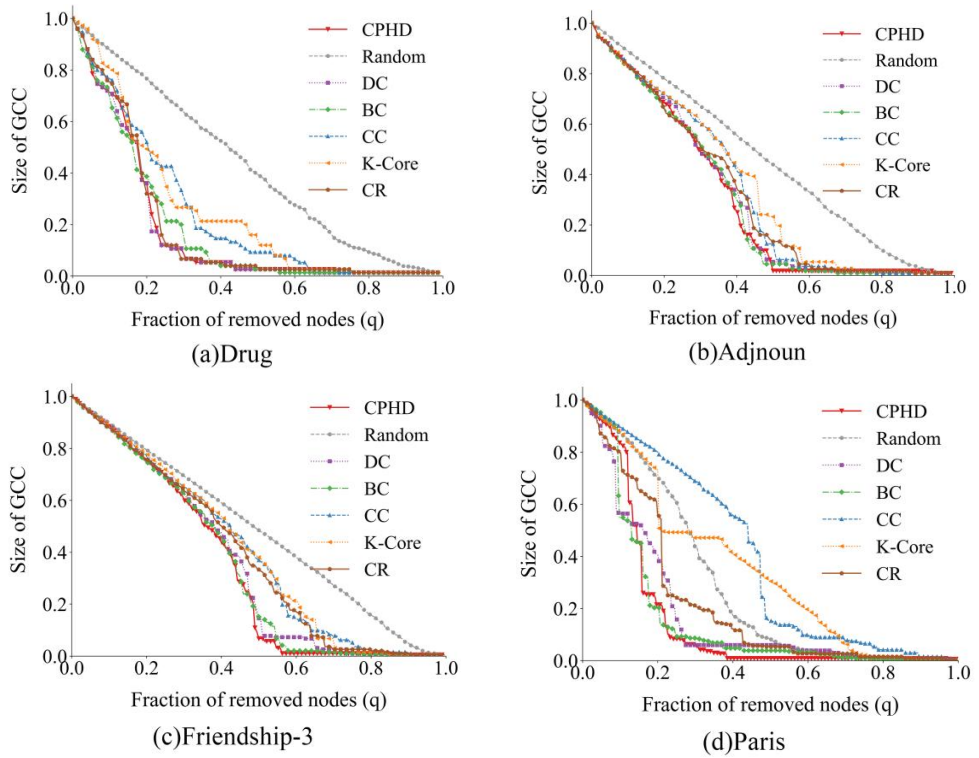


Fig. 8. Changes in giant connected components of seven node importance metrics for four real network node removals

Table 2. The Robustness of four real-world networks under seven metrics

Networks	Random	DC	BC	CC	K-core	CR	CPHD
Drug	0.4309	0.1670	0.1769	0.2355	0.2467	0.1796	0.1697
Adjnoun	0.4489	0.2926	0.2864	0.3230	0.3408	0.3080	0.2851
Friendship-3	0.4811	0.3499	0.3390	0.3952	0.3970	0.3831	0.3325
Paris	0.2770	0.1760	0.1610	0.3905	0.3465	0.2175	0.1568

4.2. Propagation Validation Analysis

To further verify CPHD's effectiveness in evaluating propagation influence, the SIR model simulates information dissemination, while Kendall's Tau coefficient quantifies the consistency between CPHD rankings and those from traditional centrality metrics.

4.2.1. SIR model

The Susceptible-Infected-Recovered (SIR) model(Changfeng Zhu, Jia, Wang, Fang, & Cheng, 2025), a classic epidemic propagation model, is widely used to evaluate node importance in information dissemination. Nodes are categorised into three states: Susceptible (S), Infected (I), and Recovered (R). Initially, only a small number of seed nodes are infected (I), with all others susceptible (S). Infected nodes can infect their neighboring nodes with an infection probability of β, causing these neighbors to transition to the infected state. Subsequently, infected nodes change to the recovered state (R) with a recovery probability of γ. Once a node enters the recovered state, it can no longer be infected. The simulation process continues until no new infected nodes emerge in the network. At this point, the number of recovered nodes reflects the influence scope of the seed nodes across the network.

4.2.2. Kendall correlation coefficient

In propagation validation, the SIR model calculates the number of ultimately recovered nodes when each node serves as the initial infection source, measuring propagation influence. Kendall's Tau coefficients are then computed between the CPHD rankings, CR rankings, traditional centrality rankings, and SIR-based propagation influence rankings, thereby comprehensively evaluating the consistency and discriminative power of each centrality measure in capturing node propagation significance.

Kendall's rank correlation coefficient is a non-parametric statistic measuring monotonic correlation between two variables, ranging over [-1, 1]. Higher values indicate greater ranking consistency, where 1 implies complete consistency, -1 complete opposition, and 0 no correlation. Consider two sequences, X and Y, related to all N nodes in a network, where $X = (x_1, x_2, \cdots, x_N)$ and $Y = (y_1, y_2, \cdots, y_N)$, along with N ordered pairs $(x_1, y_1), (x_2, y_2), \cdots, (x_N, y_N)$ generated by these nodes. For any two node pairs (x_i, y_i) and (x_j, y_j), if either $x_i > x_j$ and $y_i > y_j$ or $x_i < x_j$ and $y_i < y_j$, they are considered concordant. Otherwise, they are regarded as discordant. The calculation method for Kendall's rank correlation coefficient τ is as follows:

$$\tau = \frac{(n_c - n_d)}{\sqrt{(N(N-1)/2) \times (t_X + t_Y)}} \tag{7}$$

Where, n_c and n_d represent the number of concordant pairs and discordant pairs, respectively. t_X is the number of node pairs where $x_i = x_j$ and $y_i \neq y_j$; t_Y is the number of node pairs where $x_i \neq x_j$ and $y_i = y_j$. Additionally, if both $x_i = x_j$ and $y_i \neq y_j$ or both $x_i \neq x_j$ and $y_i = y_j$, then this node pair is not counted in either n_c or n_d.

4.2.3. Analysis of validation results

The four traditional metrics, DC, BC, CC, and K-core, along with the CPHD and CR, were applied together with the SIR model to the Drug, Adjnoun, Friendship-3, and Paris networks. Kendall's Tau correlation coefficients were calculated for these metrics under different infection probabilitiesβ.

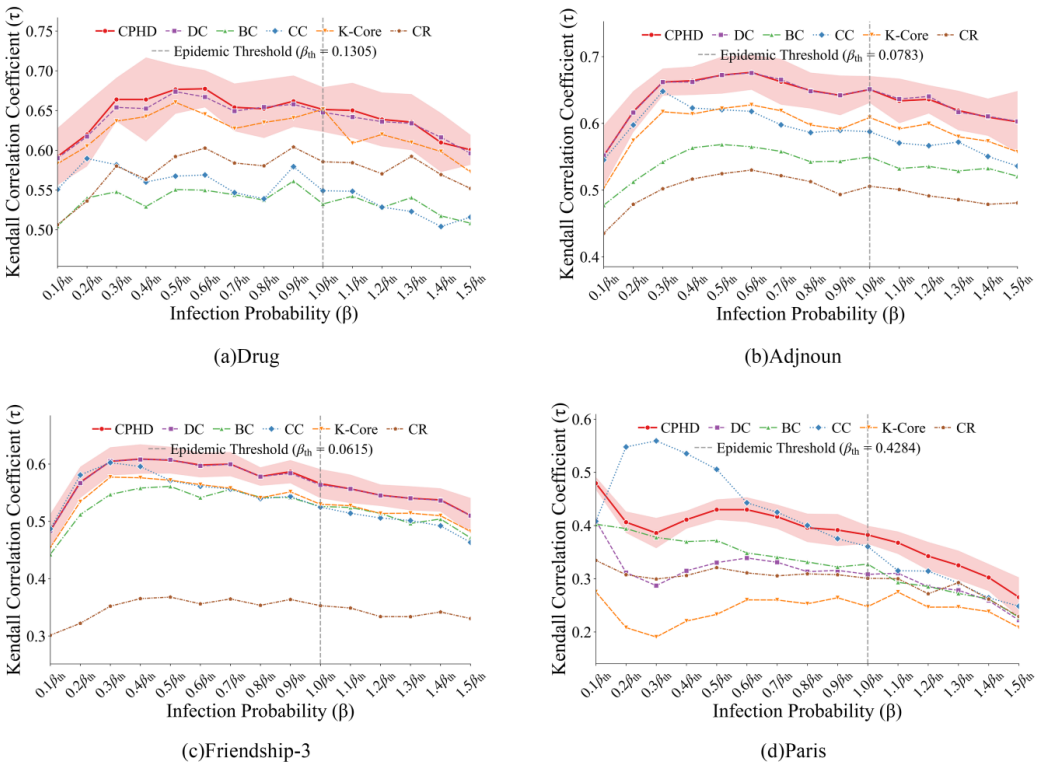
To enable the epidemic to spread rapidly across the network, the infection probability must surpass the epidemic propagation threshold β_{th}. In the experimental parameter settings, the recovery probability γ is set to 0.01. The formula for calculating the epidemic propagation threshold $\beta_{th}$is given by: $\beta_{th} = \frac{\langle k \rangle}{(\langle k^2 \rangle - \langle k \rangle)}$, where $\langle k \rangle$ and $\langle k^2 \rangle$ represent the first-order moment and the second-order moment of the average degree, respectively.

We further analyze the relationship between the infection probability β and the correlation coefficients by expressing β and the relative infection intensity in multiples of the transmission threshold β_{th}. Specifically, β varies from $0.1\beta_{th}$ to $1.5\beta_{th}$with a step size of $0.1\beta_{th}$. For each infection probability β, the full node ranking procedure is independently repeated 10 times. Within each repetition, every node is evaluated across 20 independent SIR propagation simulations, and the final Kendall's τ coefficient is reported as the arithmetic mean of the 10 repetitions. The shaded region surrounding the CPHD curve corresponds to ± 1 sample standard deviation of the 10 repeated measurements, which quantifies the fluctuation level of ranking consistency. All experiments are executed with a fixed random seed to guarantee full reproducibility of all simulation results.The

Kendall's Tau correlation coefficients under different infection probabilities are shown in Figure 9.

Across the four real-world networks, CPHD achieves relatively high τ values over most infection-probability intervals, especially near the epidemic threshold (β_{th}), where it exhibits the strongest agreement with SIR-based influence rankings. DC performs comparably on the smaller networks (Drug and Adjnoun) but degrades more sharply on larger networks as β increases. BC shows peak consistency only in a narrow low-β region on Paris, failing to maintain robustness across the full range. CR yields the weakest overall correlation: on Friendship-3 it remains substantially below all other metrics, and on the other networks it also trails CPHD by a large margin. The consistently narrow standard-deviation band around CPHD further confirms that its advantage is stable rather than an artifact of a single run. These results indicate that relying solely on local cycle counts fails to capture the nuanced topological richness provided by higher-order persistent-homology features, underscoring the superiority of the CPHD approach in identifying influential spreader.

Table 3 presents the average Kendall's Tau coefficients of the four studied networks under different infection probabilities. Overall, CPHD achieves the optimal comprehensive performance among all compared metrics: it obtains the highest correlation coefficient under the vast majority of β conditions, and maintains a distinct performance advantage across most of the infection probability range.



(a)Drug (b)Adjnoun

(c)Friendship-3 (d)Paris

Fig. 9. Changes of τ values of six algorithms under different infection probabilities

Table 3. Average τ of four networks under different β

β	DC	BC	CC	K-core	CR	CPHD
$0.1\beta_{th}$	0.5087	0.4567	0.4977	0.4539	0.3944	0.5266
$0.2\beta_{th}$	0.5279	0.4896	0.5790	0.4805	0.4111	0.5530
$0.3\beta_{th}$	0.5520	0.5037	0.5978	0.5054	0.4334	0.5791
$0.4\beta_{th}$	0.5593	0.5051	0.5785	0.5132	0.4379	0.5868
$0.5\beta_{th}$	0.5710	0.5129	0.5661	0.5218	0.4514	0.5964
$0.6\beta_{th}$	0.5696	0.5011	0.5477	0.5243	0.4499	0.5955
$0.7\beta_{th}$	0.5614	0.4996	0.5315	0.5160	0.4439	0.5832
$0.8\beta_{th}$	0.5485	0.4884	0.5163	0.5066	0.4389	0.5688
$0.9\beta_{th}$	0.5499	0.4921	0.5219	0.5119	0.4422	0.5705
$1.0\beta_{th}$	0.5426	0.4838	0.5055	0.5095	0.4362	0.5625
$1.1\beta_{th}$	0.5363	0.4730	0.4871	0.5007	0.4335	0.5521
$1.2\beta_{th}$	0.5266	0.4657	0.4788	0.4949	0.4168	0.5407
$1.3\beta_{th}$	0.5173	0.4595	0.4721	0.4876	0.4261	0.5300
$1.4\beta_{th}$	0.5056	0.4541	0.4527	0.4799	0.4129	0.5147
$1.5\beta_{th}$	0.4828	0.4319	0.4409	0.4552	0.3981	0.4946

It is worth noting that CPHD does not achieve complete dominance in every single scenario: near the two thresholds of $\beta = 0.2\beta_{th}$ and $\beta = 0.3\beta_{th}$, the correlation coefficient of betweenness centrality (CC) is slightly higher than that of CPHD. Even so, CPHD remains the metric with the best stability performance across the full range of infection probabilities, and it demonstrates both overall accuracy and robustness when characterizing the propagation influence of nodes.

4. Case Study

a. Data Sources and Network Model Construction

To validate the proposed method in complex multimodal transport scenarios, this paper uses the Belt and Road sea–rail intermodal transport network for empirical analysis. Encompassing both railway and container maritime systems, this network features extensive cross-regional coverage, tightly coupled modes, and a complex hierarchical structure, effectively reflecting the organisational and operational characteristics of real-world multimodal transport networks.

This paper employs an L-space model, integrating multi-layer complex network theory, to construct a dual-layer complex network model. In this model, cities with ports or railway stations serve as nodes, while the transportation routes between these ports or stations act as edges. The network is abstracted as a heterogeneous coupled network triplet, denoted as $G =< V, E, S >$. Where, V represents the set of nodes, encompassing railway transport stations (V_r) and maritime ports (V_m); E denotes the set of edges, comprising railway transport route edges (E_r), maritime cargo transport route edges (E_m), and interlayer edges (E_t) connecting the two systems; and S signifies the set of network layers, including the railway layer (S_r) and the maritime layer (S_m). This modelling approach preserves the topological characteristics of the subsystems while abstracting the cross-network inter-layer connections as system coupling relationships, thereby capturing the heterogeneous interactions within the multimodal transport network.

The railway transportation sub-network is constructed based on the China-Europe Railway Express route data published by the China-Europe Railway Express official website, the China Railway 95306 website, and relevant transportation platforms, and it contains a total of 84 station nodes and 125 connecting edges (Available at: https://ec.95306.cn/ and https://www.crexpress.cn/zoblmenu/trainLine. Accessed: 15 October 2025). The maritime transport sub-network is constructed based on the shipping route data of the top 10 global container liner companies by capacity, as reported by Alphaliner in 2025 (Available at: https://alphaliner.axsmarine.com/PublicTop100/. Accessed: 8 September 2025). Specifically, route information from these 10 carriers is collected and compiled to derive a total of 83 shipping routes, yielding 117 port nodes and 316 connecting edges. Considering the actual interconnections between the railway and maritime transport networks, city nodes that serve as both railway stations and maritime

ports are subjected to city mapping coupling. According to statistics, seven cities appear in both types of transport systems and act as inter-layer coupling nodes, linking the railway sub-network with the maritime sub-network. Ultimately, the Belt and Road sea-rail intermodal transport network model is constructed, comprising a total of 201 nodes and 448 connecting edges. An illustration of its overall topological structure is shown in Figure 10.

In this case study, both sub-networks are abstracted as undirected and unweighted topological networks: an edge denotes the existence of a transport service between two nodes, while service frequency, capacity, cargo volume, and travel time are not encoded. This modelling choice is justified by the operational nature of both subsystems. China–Europe freight train services operate on fixed infrastructure with essentially bidirectional routes, while Belt and Road liner services are predominantly pendulum-type, also traversing the same routes in both directions. Under these conditions, an undirected graph accurately captures the route availability that CPHD analyses. The unweighted representation is primarily driven by data constraints: comprehensive and comparable operational data, such as service frequencies, capacities, and cargo flows, across all Belt and Road nodes are not publicly available and vary rapidly, so weighting from partial or heterogeneous sources would introduce substantial uncertainty. Moreover, evaluating CPHD and all benchmark metrics on the same unweighted skeleton ensures that performance differences reflect the metrics themselves rather than heterogeneous edge attributes, consistent with the comparative experiments in Section 4.

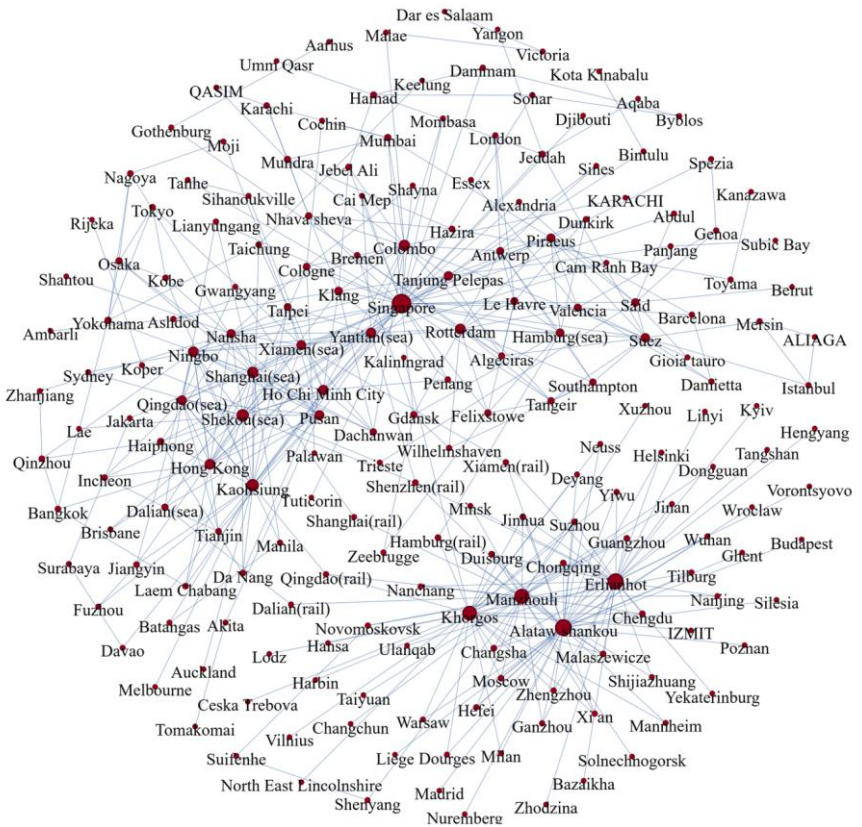


Fig. 10. Topological structure of the Belt and Road sea-rail intermodal network

Nevertheless, this abstraction introduces limitations that must be considered when interpreting the results. First, directional cargo flows are not captured: Asia–Europe trade is markedly imbalanced, with service frequencies and transit permissions varying by direction. A cycle in the undirected graph represents a structurally available detour rather than a guaranteed scheduled route, meaning the cycle-based persistence features provide an upper bound on structural redundancy rather than a catalogue of feasible rerouting options. Second, all links are treated equivalently: a high-frequency trunk service and a low-frequency feeder service contribute identically to the topology, and the filtration relies on hop-count distance rather than generalised transport cost. Consequently, the resulting importance rankings reflect structural (topological) criticality rather than flow-based or cost-based operational criticality.

b. Analysis of Topological Characteristics of the Sea-Rail Intermodal Transport Network

Firstly, an analysis is conducted on the overall topological characteristics of the Belt and Road sea-rail intermodal transport network. The statistical results reveal that the network has an average node degree of 4.3583, indicating a moderate level of overall connectivity. After fitting a function to the node degree distribution, a power-law model is obtained: $y = 197.1 - 153.6 \times 0.8^{x}$. The distribution exhibits its truncated power-law characteristics, as illustrated in Figure 11, suggesting a significant non-uniformity in the connection relationships among nodes. Specifically, a small number of nodes bear a large number of connections, while the majority of nodes have relatively low degrees of connectivity. This structural feature indicates that the aforementioned Belt and Road sea-rail intermodal transport network exhibits characteristics consistent with a scale-free degree distribution, with its overall connectivity heavily reliant on nodes with high degrees of connectivity. The failure of key nodes may thus have a substantial impact on network performance.

The average network distance$L$, refers to the mean value of the sum of distances between all pairs of nodes, reflecting the degree of separation among nodes. The distribution of distances between nodes in the Belt and Road sea-rail intermodal transport network is shown in Figure 12. It can be observed that the shortest path distances between node pairs in this network exhibit characteristics approximating a normal distribution. Statistical results indicate that node pairs with a shortest path length of 4 account for 33.6%, and approximately 93.2% of node pairs have a shortest path length of no more than 6, demonstrating good overall accessibility within the network. Further calculations reveal that the average path length of the network is 3.7148, implying that, on average, container cargo needs to traverse approximately four connecting edges, corresponding to about three transfers, to travel from the starting node to the destination node within the network, indicating relatively high overall transport efficiency. Specifically, the average path length of the railway transport sub-network is 2.6952, while that of the maritime transport sub-network is 3.3427. This suggests that, under the same scale conditions, the railway transport network has structurally shorter transport paths, with cargo requiring an average of only about two transfers to complete point-to-point transport, highlighting the efficiency and convenience of railway transport within the multimodal transport system.

Random networks typically show a low clustering coefficient and short average path length, whereas small-world networks exhibit both high clustering and short path length. For comparison, an Erdős–Rényi random network$G(n,p)$ of the same scale ($n = 201, p = 0.03$) was constructed, where each node pair is connected independently with probability$p$ and the edge probability is incrementally raised until the network is connected(Newman, 2002). The results are shown in Table 4.

Table 4. Comparison of topological properties between the sea-rail multimodal transport network and random network

Network	N	L	C
Sea-rail multimodal transport network	201	3.7148	0.2735
Random network	201	3.0872	0.0320

Both networks have an average path length below 6, consistent with the 'six degrees of separation' theory, indicating good overall accessibility. However, the sea–rail intermodal network achieves a clustering coefficient of 0.2735, significantly higher than the random network. This combination of high clustering and short path length suggests the presence of small-world characteristics in the Belt and Road sea–rail intermodal transport network.

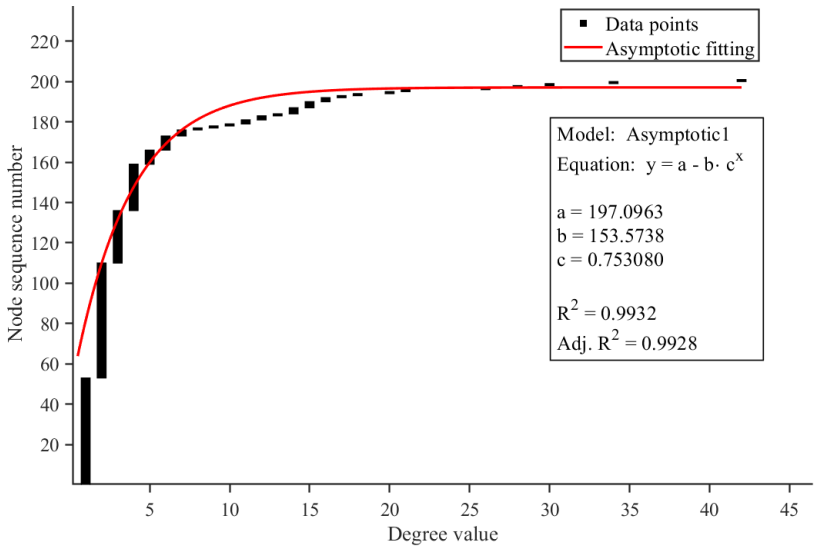


Fig. 11. Node degree distribution of the Belt and Road sea-rail multimodal transport network

c. Resilience Analysis of the Belt and Road Sea-Rail Intermodal Transport Network Under Deliberate Attacks

To evaluate the structural stability and functional retention of the Belt and Road sea–rail intermodal network under node failures, this paper simulates deliberate attacks (based on CPHD, the cycle-based metric CR, DC, BC, CC, and K-core) and random attacks. CR is included as an advanced cycle-based benchmark that ranks nodes according to their involvement in network cycles, so that the value of higher-order loop information for structural resilience assessment is explicitly tested in the comparison. Structural resilience is assessed from three perspectives: connectivity backbone preservation, structural fragmentation, and transport efficiency. This assessment employs four indicators, namely the proportion of the largest connected subgraph (GCC), the average size of non-main components, global network efficiency, and the number of connected components. The corresponding results are presented in Figure 13

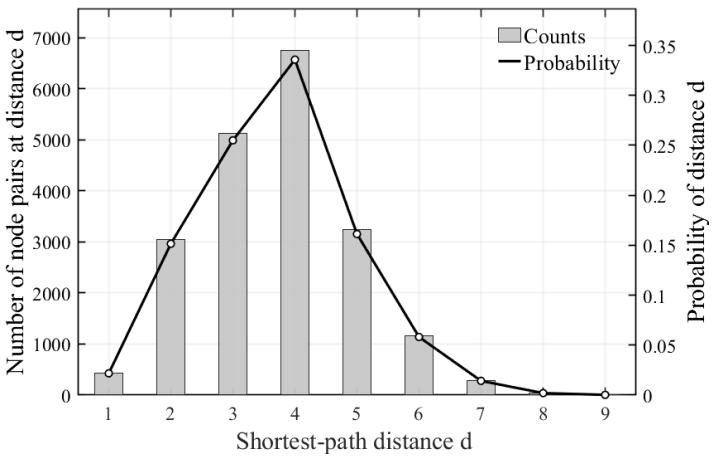
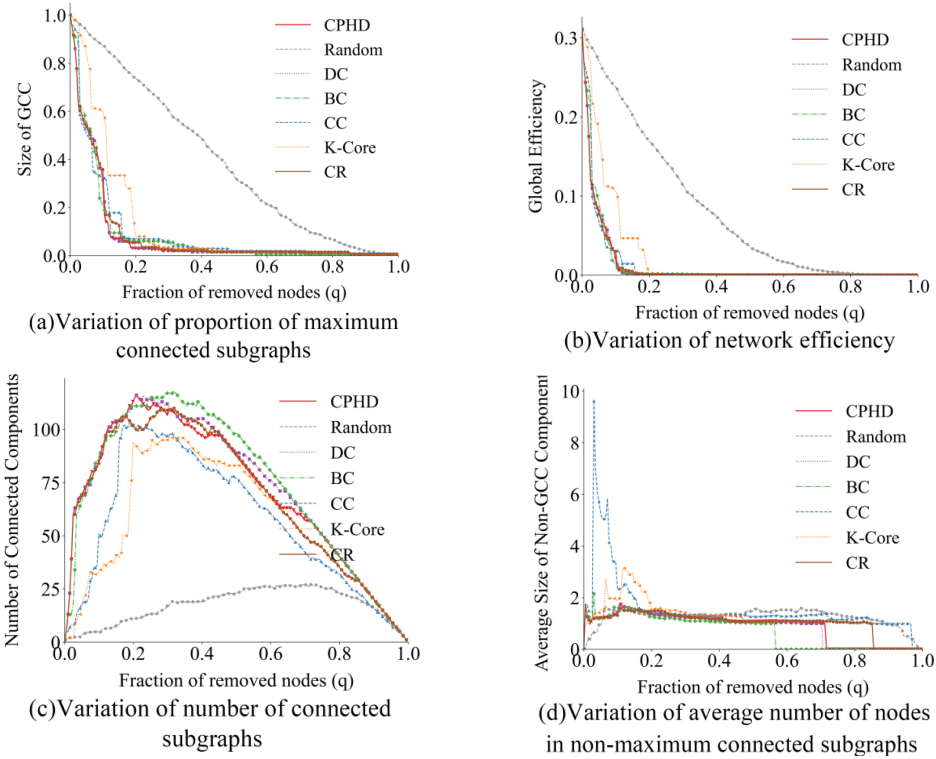


Fig. 12. Distribution of shortest-path distances between node pair



(a)Variation of proportion of maximum connected subgraphs

(b)Variation of network efficiency

(c)Variation of number of connected subgraphs

(d)Variation of average number of nodes in non-maximum connected subgraphs

Fig. 13. Variation of network parameters in the Belt and Road sea-rail multimodal transport network under different attack modes

Results show that CPHD-based node removal inflicts the most severe damage on network connectivity. When approximately 13% of high-CPHD nodes are removed, the largest connected subgraph drops below 10% of its initial size (Figure 13a), and global network efficiency falls below 10% (Figure 13b). The number of connected components rises rapidly, peaking at 117 when 22% of nodes are removed, while the average size of non-main components remains below 2 (Figures 13c–13d). These findings confirm that CPHD-identified nodes are critical for maintaining the connectivity backbone, suppressing fragmentation, and preserving transport efficiency—their failure triggers rapid network degradation.

Notably, CR produces the strongest destructive impact among the benchmarks and its curves closely track those of CPHD: under CR-based attacks the GCC and global efficiency likewise collapse to near-zero levels by $q \approx 0.2$, and the number of connected components rises to a high early peak (approximately 110). This shows that incorporating cycle information substantially improves the identification of structural resilience-critical nodes relative to traditional centrality metrics, and it corroborates the rationale of building CPHD upon cycle structures. Nevertheless, CPHD retains a marginal but consistent advantage over CR: the collapse thresholds of the GCC and global efficiency are reached at slightly smaller removal fractions, and the fragmentation peak is higher and earlier (117 at $q \approx 0.22$ versus about 110 at $q \approx 0.25 - 0.3$). The difference arises because CR only measures whether and how often nodes participate in cycles and treats all cycles equally, whereas CPHD further distinguishes cycles by their persistence (i.e., the scale and robustness of the loops) and integrates degree information, enabling it to separate genuinely resilience-critical nodes from nodes that merely lie on many short, fragile cycles.

In contrast, traditional centrality metrics (DC, BC, CC, K-core) exert weaker destructive impacts, especially in early attack stages, as they focus on local connectivity or global position while overlooking nodes' roles in maintaining collaborative relationships, path redundancy, and disruption suppression. Among them, K-core shows the slowest early degradation, because the core-decomposition ordering is insensitive to the bridging nodes that hold the sea-rail corridors together. By integrating higher-order topological persistence with node degree, CPHD more accurately identifies structural resilience-critical nodes, demonstrating clear advantages in disruption efficiency and robustness.

d. Results of Key Node Identification and Strategies for Enhancing Network Resilience

Building on the network structural resilience analysis, this paper further systematically reviews the key nodes identified through CPHD. By integrating the spatial distribution characteristics and transport organisation structure of the Belt and Road sea–rail intermodal transport network, it analyses the structural roles and mechanisms of different types of key nodes within the network, and on this basis discusses possible directions for structural resilience enhancement from a topological perspective. It should be emphasised that, as discussed in Section 5.1, these discussions are derived solely from the undirected and unweighted structural model and do not incorporate investment cost, operational feasibility, or institutional constraints; they are therefore intended as reference directions for planners and subsequent detailed studies rather than directly applicable policy prescriptions.

To compare the differences in node identification across various metrics within the multimodal transport network, Table 5 presents the top 10 nodes ranked by importance under the six metrics. Overall, the rankings generated by CPHD differ from those of the other metrics to varying degrees, with the largest disparities observed for BC, CC, and K-core, indicating that CPHD offers a distinct analytical perspective in assessing node importance compared to conventional metrics. Specifically, CPHD not only identifies core port nodes with strong radiating capabilities in the maritime network, such as Singapore, Kaohsiung, Shanghai, and Hong Kong, but also ranks railway port nodes like Alataw, Erenhot, Horgos, and Manzhouli at the forefront. In contrast, metrics like CC and K-core tend to favour port nodes with larger connection scales or relatively central locations, while falling short in identifying railway hubs that facilitate sea-rail connections, cross-border transitions, and regional bridging functions.

The cycle-based metric CR yields a top-10 list that largely coincides with that of CPHD: the two rankings share eight nodes, including an identical top five (Singapore and the four railway border nodes). Because CR relies on cycle information alone, this agreement provides independent cross-validation, from a purely cycle-based perspective, that loop structures are the key higher-order information underlying the identification of these corridor-bridging nodes. The remaining discrepancies concern mainly the hub ports. CR places Rotterdam and Ningbo in the top 10, whereas CPHD retains Shanghai and Hong Kong, reflecting the additional discrimination introduced by CPHD's persistence weighting of cycles and its integration with degree information.

Table 5. Top 10 nodes in node importance ranking under six metric

Rank	Metric					
	CPHD	**DC**	**BC**	**CC**	**K-core**	**CR**
1	Singapore	Singapore	Singapore	Singapore	Qingdao	Singapore
2	Alataw	Alataw	Alataw	Shanghai	Shanghai	Alataw
3	Erlianhot	Erlianhot	Xiamen	Qingdao	Ningbo	Erlianhot
4	Khorgos	Khorgos	Hamburg	Shekou	Xiamen	Khorgos
5	Manzhouli	Manzhouli	Manzhouli	Xiamen	Yantian	Manzhouli
6	Kaohsiung	Kaohsiung	Khorgos	Hamburg	Singapore	Rotterdam
7	Shekou	Shekou	Erlianhot	Kaohsiung	Nansha	Colombo
8	Colombo	Colombo	Qingdao	Yantian	Colombo	Kaohsiung
9	Shanghai	Shanghai	Kaohsiung	Hong Kong	Hong Kong	Shekou
10	Hong Kong	Ningbo	Shanghai	Ningbo	Pusan	Ningbo

For the Belt and Road sea-rail intermodal transport network, nodes such as Alataw, Erenhot, Horgos, and Manzhouli may not always rank highest under traditional centrality metrics, yet they serve as crucial hubs connecting inland railway corridors with the international maritime system, playing a vital role in maintaining the continuity of sea-rail transport corridors and enabling cross-regional collaborative transport. The higher rankings assigned to these nodes by CPHD indicate that, by incorporating higher-order topological persistence features, the metric can more effectively identify key nodes in the multimodal transport network that simultaneously provide structural support and facilitate functional transitions. Meanwhile, port nodes like Singapore, Kaohsiung, and Shanghai remain highly ranked under CPHD, indicating that the metric can account for both core maritime hubs and sea-rail nodes, thereby aligning more closely with the actual organisational characteristics of the multimodal transport network. Furthermore, Table 6 presents the top 30 nodes ranked by importance in the Belt and Road sea-rail intermodal transport network, as identified using the CPHD metric. It is evident that these high-value nodes exhibit significant characteristics in terms of both spatial distribution and node type: spatially, they are primarily concentrated along the main Asia-Europe multimodal transport corridors and at key junctures between maritime and land transport; in terms of node type, they encompass railway border stations, core ports, and hub cities for sea-rail intermodal transport. This indicates that the key nodes identified by CPHD are not limited to highly connected nodes within a single transport subsystem but rather focus on nodes that provide support for cross-regional transport organisation and intermodal connectivity. This structural interpretation is further supported by the agreement between CPHD and the cycle-based metric CR at the top of the ranking (Table 5), which suggests that persistent cycle structures, rather than connection scale alone, underlie the importance of these nodes.

The importance of these nodes does not solely stem from their connection scale or advantage in shortest paths but is more reflective of their structural roles in maintaining alternative routes, supporting local redundancy, and facilitating coordination among multiple transport subsystems. Consequently, within the topological model, the failure of such nodes would simultaneously weaken multiple critical transport corridors and local collaborative structures. Combining this with the resilience analysis results from Section 5.3, it can be observed that in the simulated attack scenarios, the removal of nodes with high CPHD values typically leads to the rapid collapse of the connectivity backbone in the early stages of network evolution, further indicating that this metric can effectively identify key nodes that uphold the overall structural stability of the multimodal transport network. To delineate the structural roles of key nodes across different spatial scales and transport subsystems, this paper further conducts a classified analysis of important nodes in the Belt and Road sea-rail intermodal transport network from two dimensions: spatial scale and transport subsystem type. Spatially, nodes are divided into those within China and those in the Asian/European regions; at the subsystem level, nodes are categorised into the maritime transport subsystem and the railway transport subsystem. Top 10 nodes ranked by importance under each classification are presented in Table 7.

Table 6. Top 30 nodes ranked by importance in the Belt and Road sea-rail multimodal transport network

Rank	Node	CPHD	Rank	Node	CPHD	Rank	Node	CPHD
1	Singapore	0.7155	11	Ningbo	0.2430	21	Piraeus	0.1610
2	Alataw	0.5701	12	Hochiminh	0.2286	22	Nansha	0.1594
3	Erlianhot	0.4831	13	Qingdao	0.2274	23	Klang	0.1439
4	Khorgos	0.4455	14	Rotterdam	0.2258	24	Said	0.1268
5	Manzhouli	0.4065	15	Pusan	0.2115	25	Felixstowe	0.1110
6	Kaohsiung	0.3252	16	Yantian	0.2078	26	Le Havre	0.0959
7	Shekou	0.3136	17	Xiamen	0.2071	27	Dalian	0.0948
8	Colombo	0.2729	18	Suez	0.1924	28	Taipei	0.0932
9	Shanghai	0.2575	19	Hamburg	0.1768	29	Dunkirk	0.0793
10	Hong Kong	0.2455	20	Tanjung Pelepas	0.1751	30	Cai Mep	0.0792

Table 7. Top 10 nodes based on different classification

Rank	China		Asia/Europe		Maritime Subsystem		Railway Subsystem	
	Node	CPHD	Node	CPHD	Node	CPHD	Node	CPHD
1	Alataw	0.5701	Singapore	0.7155	Singapore	0.7155	Alataw	0.5701
2	Erlianhot	0.4831	Colombo	0.2729	Kaohsiung	0.3252	Erlianhot	0.4831
3	Khorgos	0.4455	Hochiminh	0.2286	Shekou	0.3136	Khorgos	0.4455
4	Manzhouli	0.4065	Rotterdam	0.2258	Colombo	0.2729	Manzhouli	0.4065
5	Kaohsiung	0.3252	Pusan	0.2115	Shanghai	0.2575	Shekou	0.3136
6	Shekou	0.3136	Suez	0.1924	Hong Kong	0.2455	Shanghai	0.2575
7	Shanghai	0.2575	Hamburg	0.1768	Ningbo	0.2430	Qingdao	0.2274
8	Hong Kong	0.2455	Tanjung Pelepas	0.1751	Hochiminh	0.2286	Yantian	0.2078
9	Ningbo	0.2430	Piraeus	0.1610	Qingdao	0.2274	Xiamen	0.2071
10	Qingdao	0.2274	Klang	0.1439	Rotterdam	0.2258	Hamburg	0.1768

The analysis reveals significant differences in the structural characteristics and risk propagation patterns of key nodes across different regions and transport subsystems. Within China, key nodes are primarily concentrated at core border stations along the main corridors of China-Europe freight trains and at certain coastal hub ports. These nodes typically exhibit strong cross-system connectivity and path convergence capabilities, yet their local structures often suffer from insufficient alternative paths and low redundancy levels, relying heavily on specific critical corridors. For instance, in the simulation, when all railway border nodes within China fail simultaneously, as an extreme stress-test scenario rather than a realistic prediction, the global network efficiency rapidly declines from 0.2697 to 0.1002. This indicates that such nodes possess pronounced bottleneck characteristics and that their loss would lead, within the model, to a rapid degradation in overall network performance.

In contrast, key nodes in the Asian/European regions are more commonly represented by large comprehensive ports and inland hub cities. These nodes are typically located at terminal distribution or cross-regional transit points within the Asia-Europe multimodal transport system, deriving their importance primarily from their path integration capabilities and sea-rail connectivity functions at a regional scale. Compared to border-type nodes in China, these nodes generally exhibit higher local redundancy levels. However, due to their critical roles in cross-regional transport organisation and long-distance link connections, their failure would, in the topological model, have a stronger cross-regional propagation effect, often manifesting as a systemic decline in transport organisation efficiency and a significant reduction in the reachability of cross-regional shortest paths.

From the perspective of transport subsystems, key nodes in the railway subsystem are primarily cross-border border stations and mainline corridor nodes, displaying typical 'bottleneck-type' structural characteristics. Their failure is more likely to result in transport corridor disruptions and rapid fragmentation of connected components under the simulated node-removal scenarios. Conversely, key nodes in the maritime transport subsystem are mostly highly connected ports and shipping hubs, exhibiting a combination of 'hub-type' and 'bridging-type' characteristics. Their failure not only directly weakens network efficiency and alternative path levels in the topological model but may also amplify these effects across the entire network through sea-rail connectivity relationships. Overall, the importance of key nodes is not solely determined by connection scale or locational conditions but rather depends on their embedding within multi-scale path structures and cross-system collaborative relationships.

Based on the aforementioned key node identification and classification results, differentiated implications for enhancing the resilience of the Belt and Road sea-rail intermodal transport network can be further discussed as follows. From a topological perspective, this study provides a structure-oriented prioritization framework that identifies the critical areas requiring focused attention; the operational implementation of corresponding measures can be further explored in subsequent research with practical data.

1. Railway border-station key nodes: enhancing structural corridor redundancy. Topological analysis reveals that alternative paths around

these nodes are insufficient and corridor dependency is high. From a structural standpoint, planners may consider promoting multi-border-station coordination and the development of alternative corridors to reduce reliance on single passages, thereby mitigating the structural impact of single-point failures on network connectivity.

2. Hub port key nodes: alleviating structural concentration and strengthening port collaboration. Structural analysis indicates that connectivity is markedly concentrated in a small number of hub ports. At the structural level, diversifying dependence on single ports or channels and enhancing functional complementarity among port clusters can effectively reduce the network's exposure to localized disruptions.
3. Cross-system coupling key nodes: prioritizing transshipment interfaces in subsequent planning. Urban nodes serving as rail-sea intermodal points structurally bridge the two subsystems, and their failure may simultaneously compromise both. Establishing cross-system operational monitoring and emergency response mechanisms is conducive to containing cascading effects that are structurally possible; the quantification of actual propagation dynamics can be further addressed in subsequent research incorporating operational data.

5. Conclusions

This paper proposes a node importance metric, CPHD, which integrates persistent topological features of cycle structures with node degree information. By constructing a multi-scale filtration process on the second-order neighbourhood, CPHD extracts persistent cycle-structure characteristics and combines them with node degree to comprehensively characterise node importance, addressing the limitation of traditional centrality metrics in capturing higher-order topological information. Empirical studies on multiple real-world networks and the Belt and Road sea-rail intermodal transport network demonstrate CPHD's superior performance in key node identification, primarily reflected in the following aspects:

1. Connectivity disruption capability: CPHD effectively identifies structurally critical nodes. In connectivity validation experiments, the CPHD-based node removal strategy yielded the lowest robustness values across the Adjnoun, Friendship-3, and Paris networks, indicating that the nodes identified by CPHD occupy more pivotal positions within the network structure, whose failure would accelerate network disintegration.
2. Consistency with propagation impact: CPHD consistently achieved high Kendall's Tau coefficients in the Adjnoun, Friendship-3, and Paris networks, with overall performance surpassing traditional metrics such as DC, BC, CC, and K-core. This confirms that CPHD rankings exhibit the strongest agreement with the propagation influence rankings derived from the SIR model.
3. Application value to the Belt and Road sea-rail intermodal transport network: CPHD effectively captures the nodes essential for cross-system connectivity, path redundancy, and backbone integrity. Removing merely 13% of the identified key nodes reduced both the largest connected component and global efficiency to below 10% of their initial levels. Furthermore, CPHD-based attacks induced the most severe structural degradation among all benchmarks, including the cycle-based metric CR, demonstrating its effectiveness in revealing the structural vulnerability and critical weak points of the intermodal transport network within the topological framework.

Based on these key node identification results, this paper further discusses differentiated, topology-informed resilience-enhancement directions for railway border-station, hub port, and cross-system coupling nodes; these directions are derived from the structural analysis and should be validated against operational data and feasibility constraints before implementation. The proposed method offers a new structural perspective for key node identification in complex transport networks and can serve as a topological reference for prioritising attention in critical infrastructure protection and emergency preparedness in intermodal transport systems.

This study is subject to certain limitations that warrant acknowledgement.. The analysis is based on an undirected and unweighted abstraction of the intermodal network, in which service direction, frequency, capacity, and cargo flows are not represented; the identified node importance therefore reflects structural rather than operational criticality,

and the resilience-enhancement directions proposed above should be treated as topology-informed guidance to be further validated with operational data and feasibility assessments. Future work will extend CPHD to directed and weighted representations incorporating service schedules and cargo-flow data, and will evaluate the identified key nodes against real disruption scenarios.

References

1. Bag, S., Kumar, S. K., & Tiwari, M. K. (2019). An efficient recommendation generation using relevant Jaccard similarity. *Information Sciences, 483*, 53-64. https://doi.org/10.1016/j.ins.2019.01.023
2. Chami, G. F., Ahnert, S. E., Kabatereine, N. B., & Tukahebwa, E. M. (2017). Social network fragmentation and community health. *Proceedings of the National Academy of Sciences, 114*(36), E7425-E7431. https://doi.org/10.1073/pnas.1700166114
3. Chang, J. S., & Kim, S. (2022). Node centrality of North Korean Railways. *Transportation Planning and Technology, 45*(7), 573-587. https://doi.org/10.1080/03081060.2022.2147177
4. Chen, B., Hu, S., Xu, X., Wang, G., Lee, D.-H., & He, Z. (2026). A survey of multi-modal urban transportation network resilience: modeling, evaluation, and optimization. *Transportation Research Part E: Logistics and Transportation Review, 207*(March), 104634. https://doi.org/10.1016/j.tre.2025.104634
5. Chen, J., Wang, J., Xia, C., Shi, D., & Chen, G. (2025). Epidemic dynamics driven by adaptive rewiring mechanism on higher-order networks. *Chaos, Solitons & Fractals, 200*(November), 117003. https://doi.org/10.1016/j.chaos.2025.117003
6. Correia, R. B., de Araújo Kohler, L. P., Mattos, M. M., & Rocha, L. M. (2019). City-wide electronic health records reveal gender and age biases in administration of known drug–drug interactions. *NPJ digital medicine, 2*(July), 74. https://doi.org/10.1038/s41746-019-0141-x
7. Crucitti, P., Latora, V., & Porta, S. (2006). Centrality measures in spatial networks of urban streets. *Physical Review E—Statistical, Nonlinear, and Soft Matter Physics, 73*(3), 036125. https://doi.org/10.1103/PhysRevE.73.036125
8. Fan, T., Lü, L., Shi, D., & Zhou, T. (2021). Characterizing cycle structure in complex networks. *Communications Physics, 4*(1), 272. https://doi.org/10.1038/s42005-021-00781-3
9. Gao, Q., Hu, M., Yang, L., & Zhao, Z. (2024). Identification of key nodes in multi-layer heterogeneous aviation network through aggregating multi-source information. *Aerospace, 11*(8), 619. https://doi.org/10.3390/aerospace11080619
10. Guo, M., Zhao, T., & Gao, Z. (2026). Pre-disaster resource allocation based on network topology and flow features. *Transportmetrica A: Transport Science, 22*(1), 2344631. https://doi.org/10.1080/23249935.2024.2344631
11. Huang, W., Li, H., Yin, Y., Zhang, Z., Xie, A., Zhang, Y., & Cheng, G. (2024). Node importance identification of unweighted urban rail transit network: An Adjacency Information Entropy based approach. *Reliability Engineering & System Safety, 242*(February), 109766. https://doi.org/10.1016/j.ress.2023.109766
12. Huang, W., Zhang, Y., Yu, Y., Xu, Y., Xu, M., Zhang, R., . . . Liu, Z. (2021). Historical data-driven risk assessment of railway dangerous goods transportation system: Comparisons between Entropy Weight Method and Scatter Degree Method. *Reliability Engineering & System Safety, 205*, 107236. https://doi.org/10.1016/j.ress.2020.107236
13. Huang, X., Chen, J., Cai, M., Wang, W., & Hu, X. (2022). Traffic node importance evaluation based on clustering in represented transportation networks. *IEEE Transactions on Intelligent Transportation Systems, 23*(9), 16622-16631. https://doi.org/10.1109/TITS.2022.3163756
14. Huang, Y., Wang, H., Ren, X.-L., & Lü, L. (2024). Identifying key players in complex networks via network entanglement. *Communications Physics, 7*(1), 19. https://doi.org/10.1038/s42005-023-01483-8
15. Lambiotte, R., Rosvall, M., & Scholtes, I. (2019). From networks to optimal higher-order models of complex systems. *Nature physics, 15*(4), 313-320. https://doi.org/10.1038/s41567-019-0459-y
16. Latora, V., & Marchiori, M. (2001). Efficient behavior of small-world networks. *Physical review letters, 87*(19), 198701. https://doi.org/10.1103/PhysRevLett.87.198701

17. Li, J.-Y., Teng, J., & Wang, H. (2025). Measuring robustness in uncertain topologies: a study of on-demand bus networks. *Transportmetrica A: Transport Science, 21*(3), 2317783. https://doi.org/10.1080/23249935.2024.2317783
18. Lim, S., Memoli, F., & Okutan, O. B. (2024). Vietoris–Rips persistent homology, injective metric spaces, and the filling radius. *Algebraic & Geometric Topology, 24*(2), 1019-1100. https://doi.org/10.2140/agt.2024.24.1019
19. Liu, H., Tian, Z., Huang, A., & Yang, Z. (2018). Analysis of vulnerabilities in maritime supply chains. *Reliability Engineering & System Safety, 169*(January), 475-484. https://doi.org/10.1016/j.ress.2017.09.018
20. Newman, M. E. (2002). Random graphs as models of networks. *arXiv preprint cond-mat/0202208*. https://doi.org/10.48550/arXiv.cond-mat/0202208
21. Newman, M. E. (2006). Finding community structure in networks using the eigenvectors of matrices. *Physical Review E—Statistical, Nonlinear, and Soft Matter Physics, 74*(3), 036104. https://doi.org/10.1103/PhysRevE.74.036104
22. Shen, J., & Zong, H. (2023). Identification of critical transportation cities in the multimodal transportation network of China. *Physica A: Statistical Mechanics and its Applications, 628*(October), 129174. https://doi.org/10.1016/j.physa.2023.129174
23. Stamos, I. (2023). Transportation networks in the face of climate change adaptation: A review of centrality measures. *Future transportation, 3*(3), 878-900. https://doi.org/10.3390/futuretransp3030049
24. Xu, K., Liu, J., & Li, Z. (2025). Vulnerability assessments of global liner shipping network based on extended coupled map lattices. *Reliability Engineering & System Safety, 264*(December), 111306. https://doi.org/10.1016/j.ress.2025.111306
25. Xu, X., & Xu, C. (2024). Recognizing Critical Stations in Urban Rail Transit Networks Based on the PCA-TPE Method: Shanghai Metro as an Example. *Journal of Advanced Transportation, 2024*(1), 1129799. https://doi.org/10.1155/2024/1129799
26. Xu, Y., Zhao, D., Chen, J., Liu, T., & Xia, C. (2024). The nested structures of higher-order interactions promote the cooperation in complex social networks. *Chaos, Solitons & Fractals, 185*(August), 115174. https://doi.org/10.1016/j.chaos.2024.115174
27. Ye, D., Jiang, H., Jiang, Y., & Li, H. (2023). Stable distance of persistent homology for dynamic graph comparison. *Knowledge-Based Systems, 278*, 110855. https://doi.org/10.1016/j.knosys.2023.110855
28. Yiqiao, W., Xianbin, C., Fangyun, Q., & Lu Carol, T. (2022). Vulnerability analysis of the Chinese coupled aviation and high-speed railway network. *Chinese Journal of Aeronautics, 35*(12), 189-199. https://doi.org/10.1016/j.cja.2022.01.009
29. Zhang, Y., & Ng, S. T. (2021). Identification and quantification of node criticality through EWM–TOPSIS: a study of Hong Kong's MTR system. *Urban Rail Transit, 7*(3), 226-239. https://doi.org/10.1007/s40864-021-00155-6
30. Zhu, C., Jia, J., Wang, J., Fang, J., & Cheng, L. (2025). Effective passenger flow congestion propagation model for multi-mode rail transit networks. *Transportation Letters, 17*(7), 1182-1198. https://doi.org/10.1080/19427867.2024.2418215
31. Zhu, C., & Zhu, X. (2024). Vulnerability Analysis of China-Europe Railway Express Network Based on Improved Nonlinear Load-Capacity Model. *Journal of Advanced Transportation, 2024*(1), 5910244. https://doi.org/10.1155/2024/5910244